

The Influence of SnCl₄ Doping on the Electrochemical Performance of Spinel Lithium Titanate (Li₄Ti₅O₁₂) Anode Material

Keqiang Ding^{1,*}, Yongbo Zhao¹, Mian Zhao², Yuan Li¹, Jing Zhao¹, Yuying Chen¹, Qingfei Wang^{1,*}

¹College of Chemistry and Materials Science, Hebei Normal University, Shijiazhuang 050024, P.R. China

²Huihua College of Hebei Normal University, Shijiazhuang 050091, P.R. China

*E-mail: dkeqiang@263.net; wqfxt@126.com

Received: 8 July 2015 / Accepted: 29 July 2015 / Published: 26 August 2015

A sol-gel method assisted high temperature solid state reaction has been successfully employed to synthesize spinel Li₄Ti₅O₁₂/SnCl₄ composites. In this work, the effect of Ti:Sn atomic ratio was systematically investigated. The structure of the Li₄Ti₅O₁₂/SnCl₄ material was investigated by X-ray diffraction (XRD), scanning electron microscope (SEM), and the electrochemical performance was mainly studied by using cyclic voltammetry (CV), electrochemical impedance spectroscopy (EIS) and charge-discharge tests. Results of electrochemical measurements demonstrated that when the atomic ratio of Ti to Sn was 4.6:0.4, the best electrochemical performance was exhibited by the composite, delivering an initial discharge capacity of 194 mAh g⁻¹ at 0.2 C and maintaining 81.1% of its initial capacity after 20 cycles, which was remarkably superior to the pure Li₄Ti₅O₁₂ that was prepared by the same process in the absence of SnCl₄.

Keywords: Effect; SnCl₄; doping; Li₄Ti₅O₁₂; anode material; lithium-ion batteries

1. INTRODUCTION

Spinel lithium titanate (Li₄Ti₅O₁₂ (LTO)), due to its excellent properties such as the high safety, good reversibility of Li-ion insertion/extraction and near-zero structural change during charging and discharging process, has received increasing attention as a novel kind of alternative anode material to graphite in lithium-ion batteries (LIBs) [1]. Nevertheless, recent works have also revealed that the intrinsic electronic conductivity of LTO was as low as 10⁻⁹ S cm⁻¹, which could result in the larger initial capacity loss and poor rate capability, limiting the further application of LTO [2]. Therefore,

many efforts have been devoted to the exploration of novel kinds of LTO with enhanced electrochemical performance. Summarily, there are three main methods to promote the electrochemical properties of LTO, namely, reducing the particle size of LTO to shorten the diffusion path of Li-ion [3,4], doping with metal or non-metal ions into LTO to modify the structure of LTO [5], coating or blending with conductive materials to enhance the electronic conductivity of LTO [6]. In other words, exploring novel methods to fabricate LTO-based anode materials of LIBs is in progress. For example, Wang et al. [7] reported that dual-phase $\text{Li}_4\text{Ti}_5\text{O}_{12}\text{-TiO}_2$ nanocrystallines could be prepared by a hydrothermal process combined with a subsequent heat treatment. He pointed out that the dual-phase $\text{Li}_4\text{Ti}_5\text{O}_{12}\text{-TiO}_2$ nanocrystallines were highly promising anode materials for lithium ion battery applications. Xu's group [8] synthesized La^{3+} and F^- co-doped $\text{Li}_4\text{Ti}_5\text{O}_{12}$ (LTO) anode materials via a solid state reaction, and found that $\text{Li}_{3.95}\text{La}_{0.05}\text{Ti}_5\text{O}_{11.7}\text{F}_{0.3}$ delivered a discharge capacity of 103 mAh g^{-1} at 10 C rate, whereas the LTO only showed 62.5 mAh g^{-1} . Very recently, Leu et al. [9] prepared a TiO_2 nanosheets/ SnO_2 nanoparticles composite by a hydrothermal and chemical bath deposition (CBD) methods and found that the composite electrode could exhibit a high initial discharge capacity of $2239.1 \text{ mAh g}^{-1}$ and a discharge capacity of more than 868.7 mAh g^{-1} could be maintained after 50 cycles at 0.1C in a voltage range of 1.0-3.0 V at room temperature. Xiao's group [10] recently developed a facile hydrothermal and ion-exchange route for synthesizing the self-supported dual-phase $\text{Li}_4\text{Ti}_5\text{O}_{12}\text{-TiO}_2$ nanowire arrays, and they found that the dual-phase nanowire electrode yielded superior rate capability (e.g. 135.5 mAh g^{-1} at 5 C), however, in their work, no flat charging-discharging plateau was observed.

Among these developed methods, doping metal ions into LTO was regarded, mainly owing to its simplicity, as a promising synthetic way especially for the large-scale production of LTO. As a typical kind of metal ion, Sn ion has been doped into LTO with an intention to enhance the electrochemical performance of LTO. In the previous works, SnCl_2 and SnO_2 were employed as the Sn precursors to probe the influence of Sn ions-doping on the electrochemical properties of LTO. For instance, Lai [11] prepared a $\text{Li}_4\text{Ti}_5\text{O}_{12}\text{-SnO}_2$ composite anode material, in his work, $\text{Li}_4\text{Ti}_5\text{O}_{12}$ powders were firstly immersed in the $\text{SnCl}_2 \cdot n\text{H}_2\text{O}$ solution and then $\text{NH}_3 \cdot \text{H}_2\text{O}$ was dropped into the solution with stirring to deposited Sn-oxide precipitation on $\text{Li}_4\text{Ti}_5\text{O}_{12}$. He reckoned that the synergistic interaction between $\text{Li}_4\text{Ti}_5\text{O}_{12}$ and SnO_2 could enhance the electrochemical property of LTO when the doping amount of SnO_2 was appropriate. Lee et al. [12] fabricated submicron-sized polyhedral $\text{Li}_4\text{Ti}_{5-x}\text{Sn}_x\text{O}_{12}$ materials by a single-step molten salt method using SnO_2 as the starting precursor. To the best of our knowledge, there are few studies reporting on the co-effects of Sn^{4+} and Cl^- ions on the electrochemical properties of LTO using SnCl_4 as the tin precursor.

In this study, $\text{SnCl}_4 \cdot 5\text{H}_2\text{O}$ was doped into $\text{Li}_4\text{Ti}_5\text{O}_{12}$ via a sol-gel process assisted solid-state reaction. And the effects of SnCl_4 doping on the morphology, structure and electrochemical performance of LTO anode were preliminarily probed.

2. EXPERIMENTAL

2.1. Preparation of $\text{Li}_4\text{Ti}_5\text{O}_{12}/\text{SnCl}_4$ (LTO/S) composites

Spinel $\text{Li}_4\text{Ti}_5\text{O}_{12}/\text{SnCl}_4$ (denoted as LTO/S) composite was produced by a sol-gel process

assisted solid-state reaction method. Firstly, 8.168 g of tetrabutyl titanate ($[\text{CH}_3(\text{CH}_2)_3\text{O}]_4\text{Ti}$) was dissolved in 40 ml absolute ethyl alcohol to form a solution, and at the same time, 2.04 g of lithium acetate ($\text{LiAc}\cdot 2\text{H}_2\text{O}$) and 0.35 g of tin tetrachloride ($\text{SnCl}_4\cdot 5\text{H}_2\text{O}$) were dissolved in 30 ml distilled water to form another aqueous solution. And then the tetrabutyl titanate ethanol solution was added into the aqueous solution containing $\text{LiAc}\cdot 2\text{H}_2\text{O}$ and $\text{SnCl}_4\cdot 5\text{H}_2\text{O}$ dropwise at the room temperature under stirring conditions. Consequently, a creamy white colloid solution was prepared. And then the resulting solution was transferred into an air dry oven and heated at 150 °C for about 3 hours forming a solid precursor. Lastly, the precursors were thoroughly ground in an agate mortar for about 15 min to form powders, and then, the powders were pressed into pieces by using a tablet compression machine. Finally, the obtained sample pieces were calcined at 800 °C for about 10 hours in a muffle furnace under air conditions to acquire the spinel $\text{Li}_4\text{Ti}_5\text{O}_{12}/\text{SnCl}_4$ composites. To study the influence of atomic ratio of Ti to Sn, the amount of lithium acetate was kept identical and the atomic ratios of Ti to Sn varied correspondingly to produce the $\text{Li}_4\text{Ti}_5\text{O}_{12}/\text{SnCl}_4$ composites. The samples with the atomic ratios of Ti to Sn 5:0, 4.8:0.2, 4.6:0.4, 4.4:0.6, respectively, were noted as sample a, b, c and d.

2.2. Material characterization

Fourier transform infrared spectrometry (FT-IR) measurements were carried out on a Hitachi FT-IR-8900 spectrometer (Japan). The phase purity and crystal structure of the synthesized powders were featured by using a Bruker D8 ADVANCE X-ray diffractometer (XRD) equipped with a $\text{Cu K}\alpha$ source ($\lambda = 0.154 \text{ nm}$) at 40 kV and 30 mA. The 2θ angular region between 10 and 80° was explored at a scan rate of 1°/step. Scanning electron microscopy (SEM, HITACHI, S-570) were employed to observe the morphology of as-prepared particles. Energy Dispersive X-Ray Spectroscopy (EDX) spectrum analysis were carried out on a X-ray energy instrument (EDAX, PV-9900, USA).

Electrochemical performance was examined with coin-type cells, in which lithium metal foil was used as the counter electrode. To prepare the working electrodes, the active materials, acetylene black and polyvinylidene fluoride (PVDF) were mixed in an agate mortar at a weight ratio of 8:1:1 for about 10 min, and then a proper amount of N-methyl-2-pyrrolidone (NMP) was dropwise added into the above dry mixture to form slurries. Subsequently, the slurry was casted onto an aluminum foil using a glass sheet and dried at 120 °C in vacuum oven (ZK-30AB, Longkou City Factory Furnace, China) for about 6 hours. After the evaporation of the solvent, disks with a diameter of 1.0 cm were punched out of the foil. The loadings of the active materials on each disk were kept at a similar level of about 2.8 mg.

Two-electrode half cells were assembled in a nitrogen-filled glove box (ZKX, Nanjin NanDa Instrument Plant). Two-electrode half cells contained lithium metal foil as the negative electrode, Celgard 2400 separator and an electrolyte of 1 M LiClO_4 in ethylenecarbonate (EC):diethyl carbonate(DEC):dimethyl carbonate (DMC) (2:5:11, vol.). The electrochemical cycle tests were performed using a CT-3008W-5V20mA-S4 testing system (Shen Zhen Newware Technology Ltd., China) at various rates (1 C=175 mAh g^{-1}) between 0.5 and 2.5 V at room temperature. The cyclic voltammetry (CV) and electrochemical impedance spectroscopy (EIS) measurements were conducted

by an electrochemical workstation CHI660E. The EIS analysis was performed at the amplitude of 5 mV with a frequency ranging from 100 kHz to 0.1 Hz.

3. RESULTS AND DISCUSSION

3.1 Characterization of samples

The FT-IR spectra of the resulting samples are given in Fig. 1. Evidently, similar FT-IR spectra were observed for all the samples, which indicated that all the samples had similar functional groups. According to the previous report [13], the bands appearing at 3402 cm^{-1} and 1663 cm^{-1} should be assigned to the stretching band of OH⁻ and the water bending mode, respectively. Meanwhile, a strong low frequency band positioned at about 700 cm^{-1} , as shown by the red-circled part, was exhibited in all the FT-IR spectra. It was reported that this characteristic band was originated from the symmetric stretching vibrations of the octahedral group MO_6 lattice [2]. Thus, it can be inferred from Fig.1 that all the samples prepared had similar crystal structure.

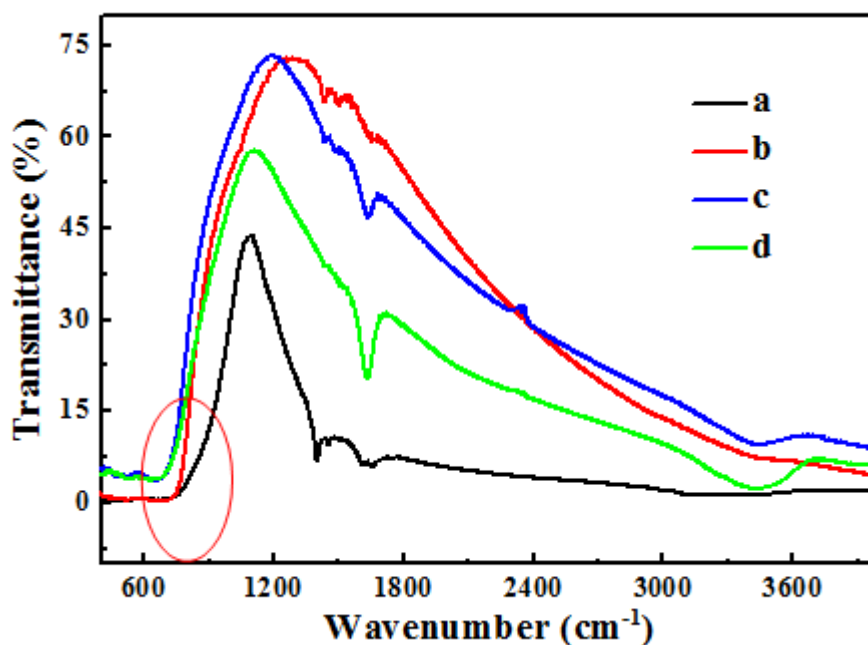


Figure 1. FT-IR spectra for the prepared samples. Spectrum a, b, c and d corresponded to sample a, b, c and d.

The XRD patterns of all the resulting samples are shown in Fig. 2. For comparison, the standard XRD pattern of LTO was also plotted in Fig.2. Apparently, the diffraction peaks in all the patterns are very sharp and well defined, which strongly indicated that all the prepared materials had a high crystalline nature. For sample a, pure LTO, all the main diffraction peaks corresponding to LTO

were exhibited clearly though the peaks belonging to TiO_2 were also displayed. In all other patterns, the typical diffraction peaks of LTO were distinctly displayed. This result effectively indicated that all the samples fabricated could be indexed as spinel lithium titanate (JCPDS Card No. 00-049-0207) and the crystal structure of the LTO was not destroyed by the SnCl_4 doping. Close inspection revealed that the intensities of the diffraction peaks for LTO decreased obviously with increasing the content of SnCl_4 , as shown by the red-circled part. And as more amounts of SnCl_4 were doped into the starting materials, the phase of SnO_2 was observed (pattern **c** and **d**). This indicated that the main components of prepared $\text{Li}_4\text{Ti}_5\text{O}_{12}/\text{SnCl}_4$ composite were $\text{Li}_4\text{Ti}_5\text{O}_{12}$ and SnO_2 .

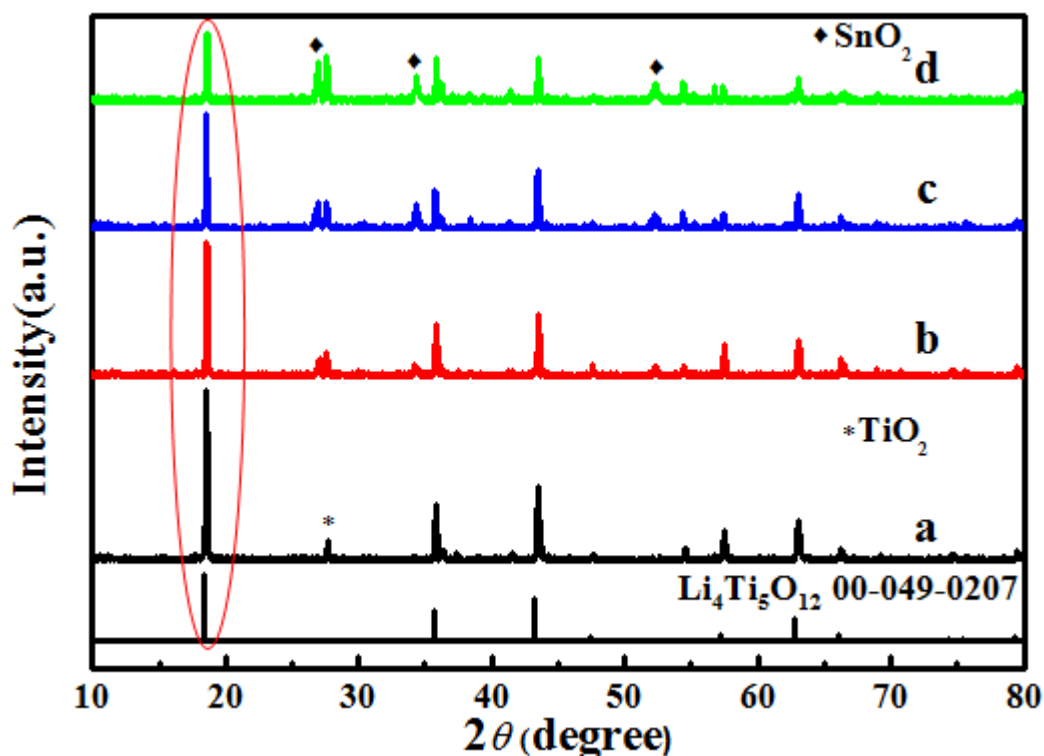


Figure 2. XRD patterns for for the prepared samples. Pattern **a**, **b**, **c** and **d** corresponded to sample **a**, **b**, **c** and **d**.

To further analyze the composition of the resultant sample, EDS analysis was conducted for all the samples as shown in Fig.3. For the SnCl_4 -doped samples, four elements of O, Ti, Sn and Cl were detected, which strongly demonstrated that SnCl_4 was really doped into the prepared $\text{Li}_4\text{Ti}_5\text{O}_{12}/\text{SnCl}_4$ composite. For instance, sample **c** was composed of 83.90% O, 14.11% Ti, 1.10% Sn and 0.85% Cl in atom content. The atomic ratio of Sn to Cl was 1.29 rather than the 0.25, implying that most amounts of Cl were volatilized in the preparation process. Meanwhile, the atomic ratio of Ti to O was rather lower than the theoretical value of 0.417 (5:12), for sample **c**, this value was as low as 0.168, which suggested that some parts of Ti and Sn elements existed in the resultant samples by means of their

oxides like TiO_2 or SnO_2 . This was advocated by the fact that the phases of TiO_2 and SnO_2 were detected in the XRD patterns of resulting samples (Fig.2).

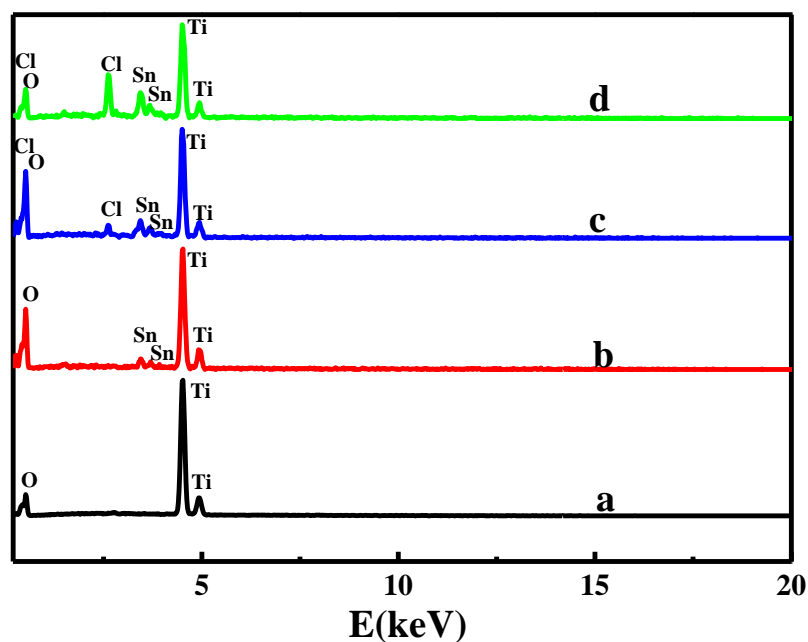


Figure 3. EDS spectra for the prepared samples. Spectrum a, b, c and d corresponded to sample a, b, c and d.

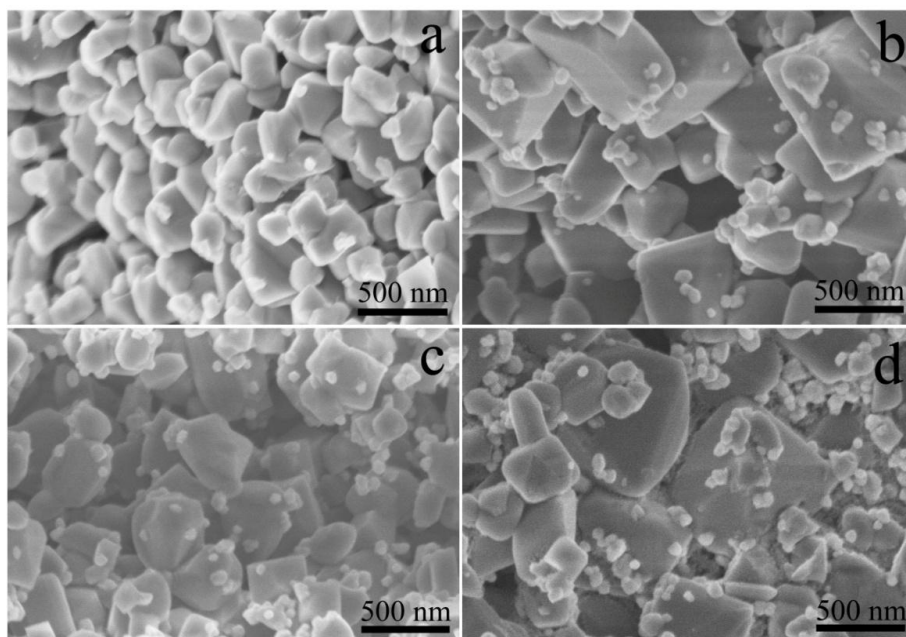


Figure 4. SEM images for the prepared samples. Image a, b, c and d corresponded to sample a, b, c and d.

All images for the prepared samples are shown in Fig.4. For the pure LTO (sample a), small irregular particles with a size of about 200 nm were exhibited. And for other samples, more larger and

regular particles were observed. The particle sizes for sample **b**, **c**, and **d** were, respectively, about 750, 375 and 875nm. That is to say, sample **c** showed the smallest particle size among the SnCl₄-doped LTO. Generally, when the loadings were identical, the reduced particle size would increase the contacting area between the electrode and electrolyte, thus, the polarization would be decreased greatly according to the Tafel equation [14]. Meanwhile, the Li⁺ diffusion path would be decreased greatly due to the reduced particle size. Therefore, sample **c** should provide satisfactory electrochemical performance when compared to other samples. Besides, the surface of these huge particles for sample **b**, **c** and **d** was coated by some small particles. These small particles may be the secondary phase, i.e., SnO₂, which was confirmed by the XRD pattern in Fig. 2.

3.2. Electrochemical properties characterization

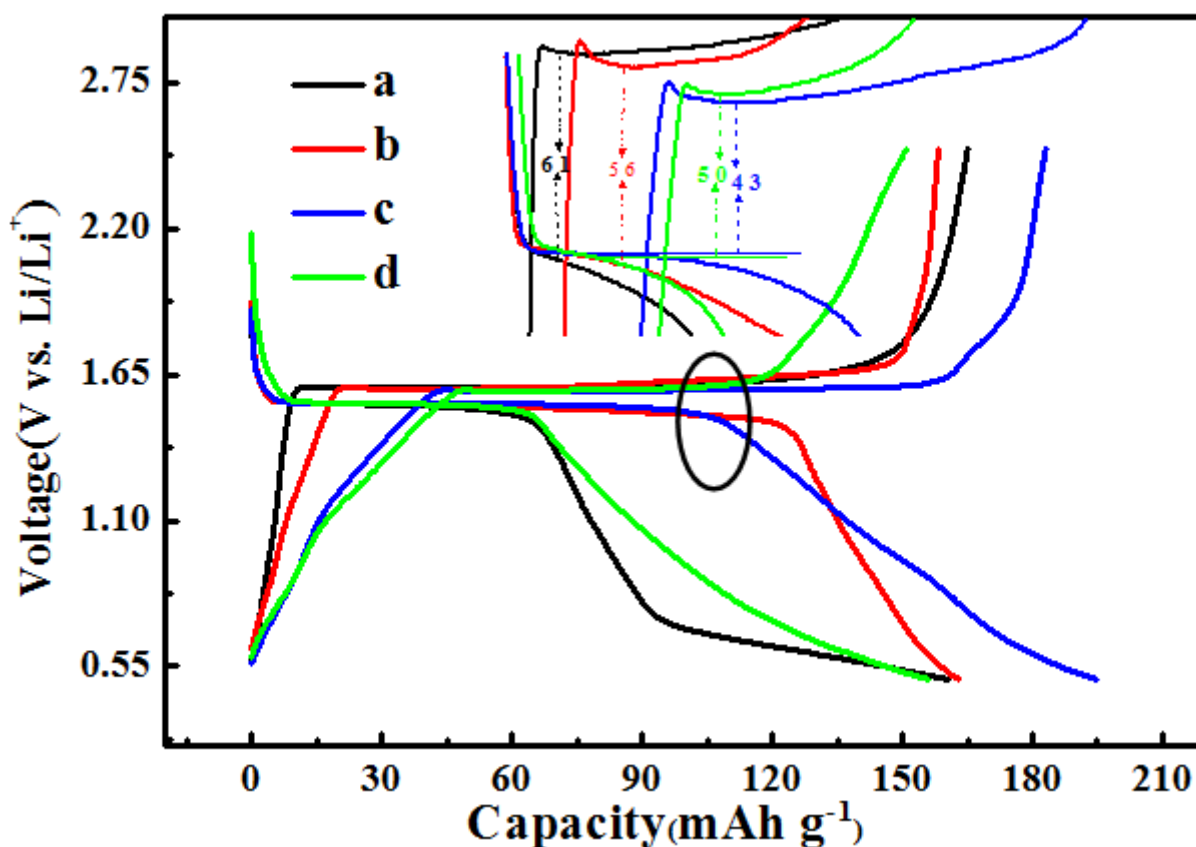


Figure 5. Charging-discharging profiles for the prepared cells obtained at 0.2C. Curves a, b, c and d corresponded to sample **a**, **b**, **c** and **d**.

The first charge/discharge profiles of the pristine LTO and LTO/SnCl₄ composites at 0.2 C rates are displayed in Fig. 5. Clearly, all electrodes showed a voltage plateau around 1.55 V. It was addressed that the presence of a voltage plateau around 1.55 V was attributed to a two-phase reaction coming from the redox couple of Ti³⁺/Ti⁴⁺ during lithium-ion extraction and insertion process [15]. Evidently, sample **b** and **c** presented longer flat plateau profile and larger plateau capacities than the pure LTO and sample **d**. The initial discharge capacities for sample **a**, **b**, **c** and **d** were 160, 163, 195

and 157 mAh g⁻¹, respectively. It should be noted that the value of 195 mAh g⁻¹ was significantly larger than the theoretical value of LTO (175 mAh g⁻¹), which substantially indicated that a proper amount of SnCl₄-doping into LTO was favorable to promote the electrochemical performance of LTO. Additionally, the value of polarization between the charge and discharge plateau was another parameter which could be employed to evaluate the reversibility of charge-discharge process. The values of polarization for sample **a**, **b**, **c** and **d** at around 90 mAh g⁻¹ were respectively, approximately 61, 56, 43 and 50mV. This result indicated that the kinetics of sample **c** was superior to other electrodes, which coincided with the fact that sample **c** delivered the largest capacity value among all the samples.

To provide insight into the cycling performances of the electrodes, the curves of discharge capacity as a function of cycling number for all the samples were plotted as shown in Fig.6. Although the discharge capacities for all the samples decreased with increasing the cycling number, the sample **c** delivered the largest capacity value throughout the whole testing period. For example, the initial discharge capacity of sample **c** was 195 mAh g⁻¹, and after 20 cycles it dropped to 159 mAh g⁻¹, maintaining 81.5% of the initial capacity. The capacity retention rates after 20 cycles for sample **a**, **b** and **d** were 76.8%, 75.5% and 76.9%, respectively. Therefore, sample **c** delivered the best cycling stability among all the electrodes.

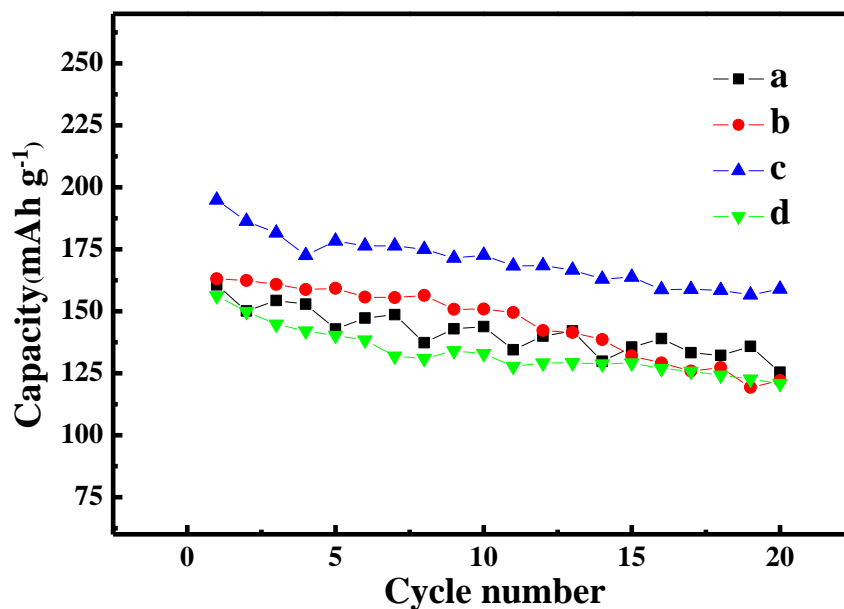


Figure 6. Cycle performance of the prepared electrodes at 0.2C rate, line a, b, c and d corresponded to sample **a**, **b**, **c** and **d**.

The rate capabilities of pristine LTO and LTO/SnCl₄ electrodes at different rates were compared as shown in Fig.7. Here, the C-rate was calculated according to the theoretical capacity of the LTO (175 mAh g⁻¹). Except for the 3C rate testing, for each rate testing, the cell was cycled for 5 cycles. Explicitly, the discharge capacity values at the same rate for all the samples increased in the

following order: sample **a** < **d** < **b** < **c**, which could be well observed as the charging-discharging rates were 3 C and 5 C. Thus, it can be concluded that sample **c** exhibited the best rate capability among the prepared samples.

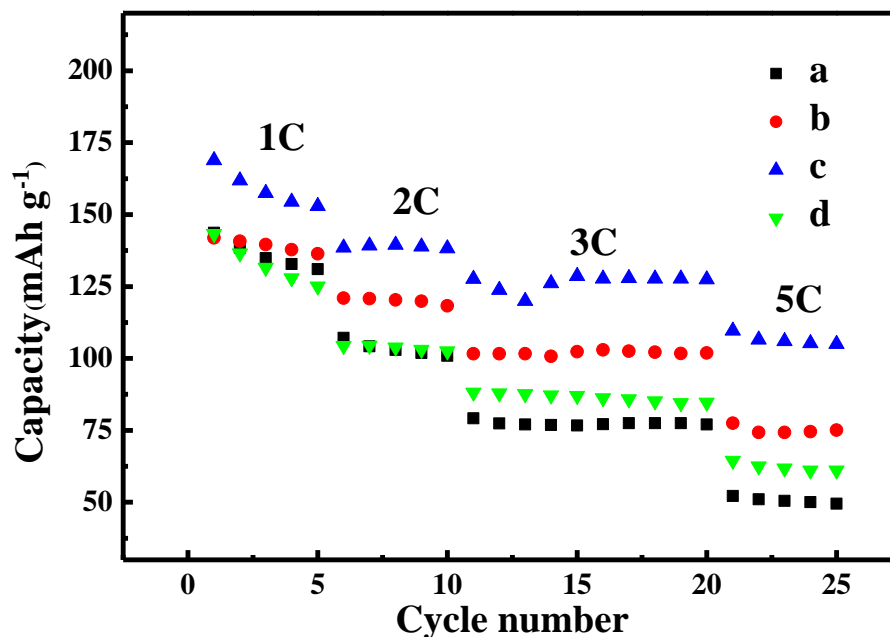


Figure 7. Comparison of the rate capabilities of all the prepared electrodes, line a, b, c and d corresponded to sample **a**, **b**, **c** and **d**.

CV curves of the battery cells assembled by SnCl₄-doped LTO at a potential scanning rate of 0.5 mV s⁻¹ in the potential range from 0.8 to 2.5 V are given in Fig.8. Apparently, pairs of well-defined redox peaks were exhibited in these three cells. Generally, the oxidation peak and reduction corresponded to the extraction process and insertion process of Li ion, respectively [16]. Obviously, sample **c** showed the largest oxidation peak current as well as the biggest reduction peak currents, indicating that sample **c** had the best electrochemical performance among all the samples. The oxidation and reduction peak potentials for sample **b**, **c** and **d** were 1.94 and 1.35V, 1.80 and 1.42V, 1.80 and 1.38V, respectively. Commonly, the value of the peak potential interval between oxidation and reduction peaks (ΔE_p , $\Delta E_p = E_{pa} - E_{pc}$, where E_{pa} and E_{pc} are the peak potentials for anodic and cathodic reaction, respectively) could be utilized as a parameter that could reflect the reversibility of an electrochemical reaction [17]. And the more broadened the peak interval, the higher the electrode polarization, thus, a smaller peak potential separation always indicates a better reversibility of a battery cell [18]. Obviously, the values of peak potential separation for sample **b**, **c** and **d** were 0.59 V, 0.38 V and 0.42 V, respectively. Thus, the reversibility for the intercalation/deintercalation process of the Li ions in sample **c** was much better than that in other SnCl₄-doped samples.

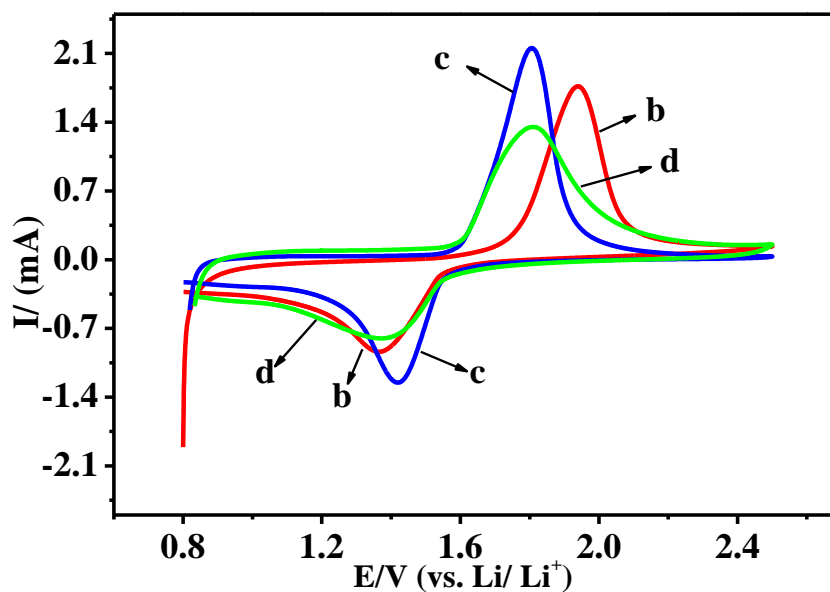


Figure 8. Cyclic voltammograms (CVs) for SnCl₄-doped LTO electrodes at a scan rate of 0.5 mV s⁻¹. Curve b, c and d corresponded to sample b, c and d.

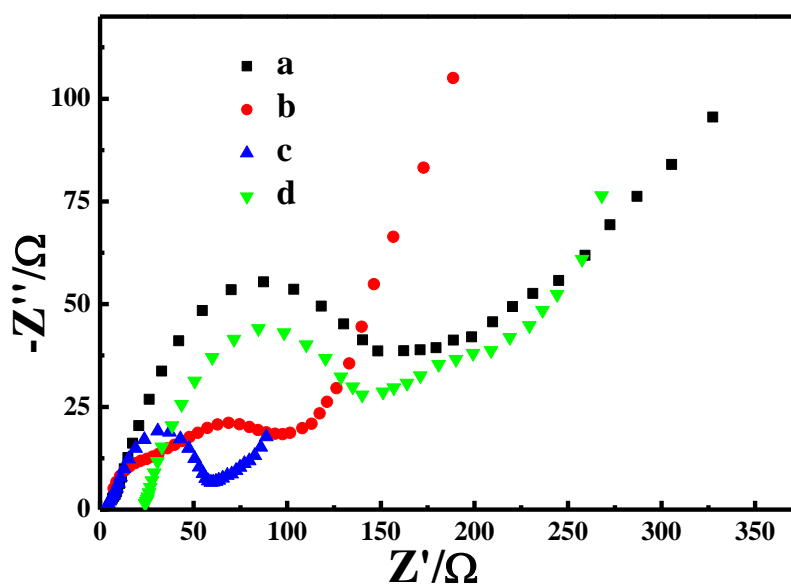


Figure 9. Nyquist plots spectra obtained at the open circuit potentials for all the prepared electrodes within frequency range of 100 kHz to 0.1Hz. Spectra a, b, c and d corresponded to sample a, b, c and d.

Electrochemical impedance spectroscopy (EIS) measurement was a powerful technique which could directly reflect the charging transfer process occurring in a half cell [19, 20]. Fig.9 shows the typical Nyquist plots for all the half cells assembled by the prepared electrode materials. Commonly, in the obtained Nyquist plots, the semi-circle appearing in the high frequency region corresponded to the charge-transfer-limited process existing at the interface of electrodes, while, the inclined line at the lower frequency region stands for the Warburg factor being associated with the diffusion-controlled

process of the Li ions in LTO [21]. And the value of the diameter for the semicircle on the Z' axis approximately amounts to the charge transfer resistance (R_{ct}). Therefore, the values of R_{ct} for sample **a**, **b**, **c** and **d** were estimated to be 208, 128, 68 and 155 Ω , respectively. In other words, the values of R_{ct} followed the decreasing order: sample **a**>**d**>**b**>**c**, which was just opposite to the order of discharge capacities exhibited at 3 C and 5 C (Fig.7). This result effectively demonstrated that the intercalation/deintercalation process of Li ion in the battery cell constructed by sample **c** was easier than that in other sample assembled cells.

How does one understand the influence of SnCl_4 on the electrochemical performance of LTO? As shown in the XRD patterns of the SnCl_4 -doped LTO, SnO_2 and TiO_2 were prepared in the resultant samples. According to the previous report, due to its high theoretical specific capacity (790 mAh g^{-1}) and low Li intercalation potential, SnO_2 has been considered as one of the most promising anode material candidates [22]. Thus, it was reasonable to think that the excellent electrochemical performance exhibited by sample **c** was partly attributed to the presence of SnO_2 . Nevertheless, as the content of SnO_2 was increased, the capacity will dropped remarkably. It was stated that during the charge-discharge process, the volume change of SnO_2 was severe which would lead to a serious pulverization of the electrode materials, generating a fast capacity fading [22]. Although TiO_2 has been extensively investigated as employed as a kind of energy storage materials, its poor electronic conductivity and sluggish lithium ion diffusion have greatly hampered its practical application [23]. Based on our former works concerning LTO, the presence of TiO_2 was detrimental to the electrochemical performance of LTO [18]. Meanwhile, on the basis of the previous works concerning the Br^- -doped LTO [24], probably some O^{2-} sites in LTO were substituted by Cl^- ions, thus, a amount of Ti ions would be converted from Ti^{4+} to Ti^{3+} for charge compensation. Consequently, the charge transfer resistance of SnCl_4 -doped LTO was reduced to some extent. Apparently, all above aspects, including the formation of SnO_2 and TiO_2 , Cl^- doping, have a strong impact on the electrochemical behavior of LTO electrode. As a result, sample **c**, having the best synergistic interaction among all the samples, delivered the best electrochemical performance among all the prepared electrodes.

4. CONCLUSION

For the first time, a spinel composite of $\text{Li}_4\text{Ti}_5\text{O}_{12}/\text{SnCl}_4$ was prepared by a sol-gel method assisted high temperature solid-state process. And the influence of SnCl_4 -doping content on the structure as well as the electrochemical performance of the resultant composite was studied preliminarily. The results demonstrated that when the atomic ratio of Ti to Sn was 4.6:0.4, the $\text{Li}_4\text{Ti}_5\text{O}_{12}/\text{SnCl}_4$ composite exhibited both the largest capacity value and the best rate capability among all the prepared samples. The best synergistic interaction was thought as the main reasons for excellent electrochemical performance exhibited by the $\text{Li}_4\text{Ti}_5\text{O}_{12}/\text{SnCl}_4$ composite (atomic ratio of Ti to Sn was 4.6:0.4). This work is believed to be beneficial for developing novel LTO-based anode materials.

ACKNOWLEDGEMENTS

This work was financially supported by the National Natural Science Foundation of China (No. 21173066), Natural Science Foundation of Hebei Province of China (No.B2015205150; No.B2011205014).

References

1. X. Li, Y. Zhou, P.. Huang, H. Peng, W. Li, M. Qu, Z.. Yu, X. Huang, Y. Chen, *Int. J. Electrochem. Sci.*, 9 (2014) 4816.
2. K. M. Yang, Y. J. Hong, S. H. Choi, B. Kyu. Park, Y. C. Kang, *Int. J. Electrochem. Sci.*, 8 (2013) 1026.
3. H. Yan, Z. Zhu, D. Zhang and W. Li, *J. Power Sources*, 219 (2012) 45.
4. F.X. Wu, X.H. Li, Z.X. Wang, H.J. Guo, Z.J. He, Q. Zhang, X.H. Xiong and P. Yue, *J. Power Sources*, 202 (2012) 374.
5. B. Zhang, Z.D. Huang, S. W. Oh and J.-K. Kim, *J. Power Sources*, 196 (2011) 10692.
6. Z. Xie, X. Li, W. Li, M. Chen and M. Qu, *J. Power Sources*, 273 (2015) 754.
7. G.-Y. Liu, H.-Y. Wang, G.-Q. Liu, Z.-Z. Yang, B. Jin and Q.-C. Jiang, *Electrochim. Acta*, 87 (2013) 218.
8. M. Ji , Y. Xu, Z. Zhao, H. Zhang, D. Liu, C. Zhao, X. Qian and C. Zhao, *J. Power Sources*, 263 (2014) 296.
9. H.-Y. Wu, M.-H. Hon, C.-Y. Kuan and I.-C. Leu, *Ceram. Int.*, 41 (2015) 9527.
10. J.-Y. Liao, V. Chabot, M. Gu, C. Wang, X. Xiao and Z. Chen, *Nano Energy*, 9 (2014) 383.
11. Y.-J. Hao, Q.-Y. Lai, Y.-D. Chen, J.-Z. Lu and X.-Y. Ji, *J. Alloy. Compd.*, 462 (2008) 404.
12. S. Sharmila, B. Senthilkumar, V.D.Nithya, K. VEDIAPPAN, C. W. Lee and R. K. Selvan, *J. Phys. Chem. Solids*, 74 (2013) 1515.
13. D.R. Simon, E.M. Kelder, M. Wagemaker, F.M. Mulder and J. Schoonman, *Solid State Ionics*, 177 (2006) 2759.
14. C. Heubner, M. Schneider and A. Michaelis, *J. Power Sources*, 288 (2015) 115.
15. S. Bach, J.P. Pereira-Ramos and N. Baffier, *J. Power Sources*, 81-82 (1999) 273.
16. K. Ding, W. Li, Q. Wang, S. Wei and Z. Guo, *J. Nanosci. Nanotechnol.* 12 (2012) 3813.
17. K. Ding, T. Okajima and T. Ohsaka, *Electrochemistry*, 75 (2007) 35.
18. G.-Q. Zhang, W. Li, H. Yang, Y. Wang, S. B. Rapole, Y. Cao, C. Zheng, K. Ding and Z. Guo, *J. New Mat. Electr. Sys.*, 16 (2013) 25.
19. K. Ding, H. Gu, C. Zheng, L. Liu, L. Liu, X. Yan and Z. Guo, *Electrochim. Acta*, 146 (2014) 585.
20. K. Ding, L. Wang, J. Li, H. Jia and X. He, *Int. J. Electrochem. Sci.*, 7 (2012) 1611.
21. T.-F. Yi, H. Liu, Y.-R. Zhu, L.-J. Jiang, Y. Xie and R.-S. Zhu, *J. Power Sources*, 215 (2012) 258.
22. Z. Yang, S. Zhao, W. Jiang, X. Sun, Y. Meng, C. Sun and S. Ding, *Electrochim. Acta*, 158 (2015) 321.
23. Z. Xiu, X. Hao, Y. Wu, Q. Lu and S. Liu, *J. Power Sources*, 287 (2015) 334.
24. Y. Qi, Y. Huang, D. Jia, S.-J. Bao and Z. P. Guo, *Electrochim. Acta*, 54 (2009) 4772.